Subthreshold photoionization of CH_3I in Ar, N_2 and CO_2

C. M. Evans[a,b], R. Reininger[a] and G. L. Findley[a,*]

[a]*Department of Chemistry, University of Louisiana at Monroe, Monroe, LA 71209, USA*
[b]*Center for Advanced Microstructures and Devices (CAMD) and Department of Chemistry, Louisiana State University, Baton Rouge, LA 70803, USA*

Abstract

We present pressure-dependent subthreshold photoionization spectra of CH_3I doped into varying number densities of the perturber gases Ar, N_2 and CO_2. The intensity of the observed subthreshold structure is discussed in terms of two different interactions, namely electron attachment and associative ionization. Effective rate constants for these two processes are analyzed, and the variation in these constants is discussed in terms of the properties of the dopant excited state.

1. Introduction

Perturber effects on the electronic structure of molecules continue to generate considerable interest using a variety of experimental techniques, including photoabsorption, photoionization and field ionization spectroscopies. Methyl iodide (CH_3I) has served as the dopant in many such studies because of the atomic-like Rydberg series and the low ionization energy ($I_1 \equiv I(^2E_{3/2}) = 9.54$ eV [1]) observed for this molecule. Perturbers have included rare gases [1-5], H_2 [4], alkanes [6], CO_2 [7], N_2 [8] and SF_6 [9,10]. Both photoabsorption and photoionization spectra have been measured, and perturber pressure effects have been analyzed for discrete and autoionizing dopant Rydberg states [1-9], as well as for subthreshold photoionization structure [3,5,7,8,10].

Photoionization spectra of CH_3I [5,10-12] and of CH_3I doped into Ar[5], Xe [3], CO_2 [7], N_2 [8] and SF_6 [10] exhibit rich subthreshold structure beginning 0.17 eV before the ionization limit I_1. From the observed energy spacing and linear energy shift (as a function of perturber number density) of the peaks, this structure has been identified as arising from high-n Rydberg states of CH_3I. This identification permits the evaluation of electron scattering lengths in highly absorbing perturber media [3,7,8,10]. (Indeed, all of the techniques mentioned above provide a high-precision adjunct [1-10] to the measurement of electron scattering lengths by low-energy electron scattering [13] and electron swarm [14] experiments.)

The low energy onset of CH_3I subthreshold ionization rules out collisional transfer of translational or rotational energy from a perturber molecule at room temperature as the ionization mechanism. Therefore, Ivanov and Vilesov [11,12] discussed three bimolecular processes leading to subthreshold structure which, for a general dopant (D)/perturber (P) system, can be symbolized as

$$D^* + P \rightarrow D^+ + P^- \quad (1)$$

$$\rightarrow [DP]^+ + e^- \quad (2)$$

* Corresponding author. Fax: + 1 318 342 1859; e-mail: chfindley@ulm.edu

$$\rightarrow R_1^+ + R_2 + e^- . \qquad (3)$$

Eq. (1) represents electron attachment [15], eq. (2) is associative ionization [15] (i.e., the Hornbeck-Molnar [16] process), and eq. (3) describes a photochemical rearrangement leading to charged particles. In their discussion of pure CH_3I (D = P = CH_3I), Ivanov and Vilesov [11,12] attributed the presence of subthreshold structure in the pure CH_3I photoionization spectra at high pressures of CH_3I to eq. (2), since the intensity was quadratically dependent upon the pressure of CH_3I and showed no temperature effect indicative of vibrational autoionization. Eq. (3), namely photochemical rearrangement leading to charged particles, was ruled out by Ivanov and Vilesov [11,12] on the basis of energetic considerations.

Recently [10], we also showed that the intensity of the subthreshold structure in pure methyl iodide depends quadratically on the CH_3I pressure (in accord with the experiments by Ivanov and Vilesov [12]), while the intensity of the subthreshold structure in CH_3I doped into SF_6 depends linearly on the SF_6 pressure. This was explained [10] by assuming that eq. (1) was saturated (i.e., independent of perturber pressure) for a highly polarizable perturber, allowing the electron attachment contribution to the photocurrent to be written as [10]

$$i_{ea} = k_1 \rho_D . \qquad (4)$$

In eq. (4) the effective rate constant k_1 is proportional to the (saturated) attachment cross section, and we have assumed for the dopant number densities that $\rho_{D^*} \propto \rho_D$ in the linear absorption regime. Likewise, the associative ionization [eq. (2)] contribution to the photocurrent can be written as [10]

$$i_{ai} = k_2 \rho_D \rho_P , \qquad (5)$$

where the effective rate constant k_2 is proportional to the associative ionization cross section, and where ρ_P is the perturber number density. In the absence of any significant photochemical contribution [i.e., eq. (3)] to the observed photocurrent, then, the subthreshold photocurrent is given by [10]

$$i = (k_1 + k_2 \rho_P) \rho_D . \qquad (6)$$

Assuming that the attachment cross-section scales linearly [15] with the principal quantum number n for the CH_3I excited state, k_1 should vary linearly with n. The parameter k_2, on the other hand, is reflective of a molecular interaction, and therefore should depend upon the excited state polarizability of CH_3I [17], which in turn scales according to n^7 [15]. For the case of CH_3I doped into SF_6 [10], we indeed found that k_1 varies linearly with n, while k_2 varies linearly with n^7. Eq. (6) also applies in the case of pure CH_3I [10], but now $\rho_P = \rho_D$, leading to

$$i = k_1 \rho_D + k_2 \rho_D^2 . \qquad (7)$$

For pure CH_3I, we again found [10] that k_1 varies linearly with n, while k_2 varies linearly with n^7.

In the present paper, we report the pressure-dependent subthreshold photoionization spectra of CH_3I doped into Ar, N_2 and CO_2, and compare these results to our previous SF_6 study [10]. In all cases, we observe a linear dependence of the photocurrent intensity upon the perturber number density, with no temperature effect. For the perturbers discussed here, however, as opposed to the strongly electron-attaching perturber SF_6, eq. (1) cannot be the mechanism leading to the photocurrent contribution represented by eq. (4). In addition, since the energy onset for subthreshold photoionization is the same for Ar, N_2 and CO_2, as will be shown below, eq. (2) is doubtful as the mechanism leading to the photocurrent contribution represented by eq. (5). In order to

model the pressure dependence of the subthreshold photoionization spectra reported here, we invoke a modification of the explanation given for subthreshold photoionization in pure CH_3I [10], namely,

$$CH_3I^* + CH_3I \xrightarrow{k_1} CH_3I^+ + CH_3I^- \quad (8)$$

$$CH_3I^* + CH_3I + P \xrightarrow{k_2} (CH_3I)_2^+ + P + e^- \quad (9)$$

As was the case in pure CH_3I (and CH_3I/SF_6), we continue to assume that the electron attachment [i.e., eq. (8)] is saturated. In line with recent electron swarm studies of halocarbons perturbed by N_2 and CO_2 [18], however, we invoke a perturber stabilization of the associative ionization step, as indicated in eq. (9). In this case, then, eq. (7) becomes

$$i = k_1 \rho_D + k_2 \rho_D^2 \rho_P . \quad (10)$$

As will be shown below, eq. (10) is sufficient to explain the pressure dependences observed in the present work.

2. Experiment

Photoionization and photoabsorption spectra were measured using monochromatized synchrotron radiation with a resolution of 0.13 nm (200 μ slits), or ~ 10 meV in the spectral range of interest. Two different experimental cells were used: Cell 1 [19] is equipped with entrance and exit MgF_2 windows and a pair of parallel plate electrodes (stainless steel, 3.0 mm spacing) oriented parallel to the incoming radiation and perpendicular to the windows, thus permitting the simultaneous recording of photoionization and transmission spectra. The light path inside the cell is 1.0 cm. Cell 2 [20] is equipped with an entrance LiF window coated with a thin (7 nm) layer of gold to act as an electrode. The second electrode (stainless steel) is placed parallel to the window with a spacing of 1.05 mm. The bodies of both cells are fabricated from copper and are capable of withstanding pressures up to 100 bar. Each cell was connected to a cryostat and heater system allowing the temperature to be controlled to within ± 1 K [19]. The applied electric field was 100 V, with the negative electrode being the LiF window in cell 2. (The reported spectra were current saturated, which was verified by measuring selected spectra at different electric field strengths.) Photocurrents within the cell were of the order of 10^{-10} A.

The intensity of the synchrotron radiation exiting the monochromator was monitored by measuring the photoemission current from a metallic grid intercepting the beam prior to the experimental cell. All photoionization spectra are normalized to this current. Transmission spectra (which are reported as absorption = 1 - transmission) were normalized both to the incident light intensity and to the empty cell transmission.

CH_3I (Aldrich Chemical Company, 99%), Ar (Matheson Gas Products, 99.9999%), N_2 (Matheson Gas Products, 99.9999%) and CO_2 (Matheson Gas Products, 99.995%) were used without further purification. The gas handling system has been described previously, as well as the procedures employed to ensure a homogeneous mixing of CH_3I with the perturber gases [6].

3. Results and discussion

Subthreshold photoionization spectra for CH_3I doped into Ar, N_2 and CO_2 (measured at the same pressure of CH_3I and the same perturber number density) are presented in Fig. 1 in comparison to the low-pressure photoabsorption spectrum of CH_3I. We have

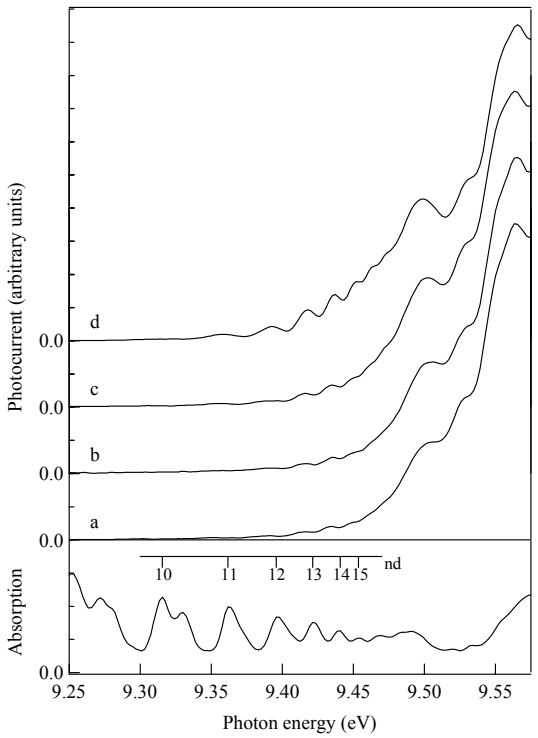

Fig. 1. Subthreshold photoionization (cell 2, 200 μ slits) of 5.0 mbar CH_3I in various perturbers (at a number density of 0.12 x 10^{19} cm^{-3}): a, Ar; b, N_2; c, CO_2; d, SF_6 [10]. Absorption of pure CH_3I (cell 1, 200 μ slits): 0.1 mbar. Each photoionization spectrum is normalized to unity at the same spectral feature above the $^2E_{3/2}$ ionization threshold.

also included our previously reported [10] CH_3I/SF_6 spectrum in this figure. (All of the photoionization spectra presented are normalized to unity at the same spectral feature above the CH_3I $^2E_{3/2}$ threshold.) From Fig. 1, one observes that the subthreshold photoionization structure correlates in all cases with the nd Rydberg states of CH_3I converging on the $^2E_{3/2}$ ionization limit, and that the intensity of the subthreshold structure increases as Ar < N_2 < CO_2 < SF_6. Representative subthreshold photoionization spectra for CH_3I doped into varying number densities of Ar are presented in Fig. 2. (The perturbers N_2 and CO_2 give rise to spectra which are qualitatively similar to those of Fig. 2. For brevity, we have not reproduced those spectra here.) As was observed for CH_3I/SF_6 [10], photoionization spectra for one dopant/perturber sample pressure, measured at different temperatures for each perturber gas, show no temperature effect on the subthreshold structure, thus ruling out vibrational autoionization as the subthreshold ionization mechanism.

We have extracted peak areas (by gaussian fits to the photoionization spectra) for the density-dependent subthreshold structure of CH_3I doped into Ar, N_2 and CO_2. These data are collected in Table 1 (CH_3I/Ar), Table 2 (CH_3I/N_2) and Table 3 (CH_3I/CO_2). Since ρ_D is constant, eq. (10) may be rewritten as

$$i = b_0 + b_1 \rho_P , \qquad (11)$$

where $b_0 = k_1 \rho_D$ and $b_1 = k_2 \rho_D^2$. These linear correlation coefficients are also collected in

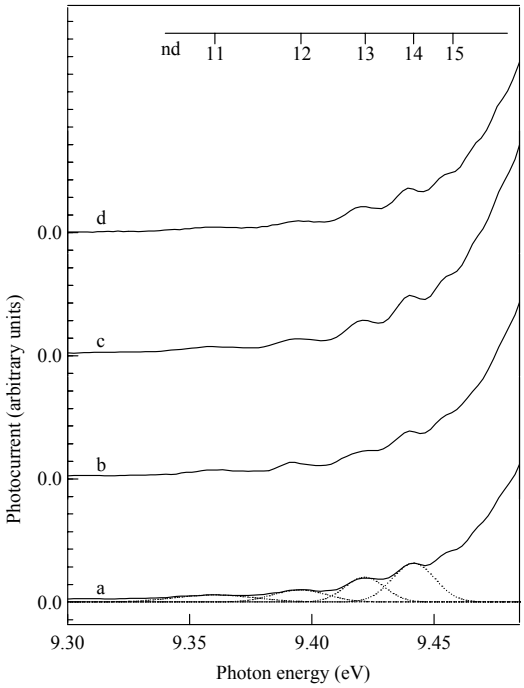

Fig. 2. Subthreshold photoionization spectra of CH_3I/Ar at 298K. Photoionization (cell 2, 200 μ slits) of 5.0 mbar CH_3I in varying Ar number densities (10^{19} cm^{-3}): a, 0.12 b, 0.24; c, 0.48; d, 1.23. Each photoionization spectrum is normalized to unity at the same spectral feature above the $^2E_{3/2}$ ionization threshold. In (a), the dotted lines are an example of the Gaussian fits used to obtain peak intensities.

Table 1
Peak areas (by gaussian fits to the photoionization spectra) for the subthreshold photoionization structure (cf. Fig. 2) of 5.0 mbar CH_3I in varying number densities ρ (10^{19} cm^{-3}) of Ar.

ρ	11d	12d	13d	14d
0.12	0.0543	0.203	0.379	0.544
0.24	0.0615	0.216	0.398	0.579
0.48	0.0722	0.255	0.449	0.676
0.73	0.0851	0.269	0.501	0.753
1.23	0.107	0.330	0.602	
Regression Coefficients				
b_0	0.0482	0.189	0.351	0.502
b_1	0.0498	0.113	0.204	0.342

The regression coefficients are for a least-squares linear fit, $b_1 \rho + b_0$, as shown in Fig. 3a.

Tables 1-3, and the photoionization peak areas are plotted versus ρ_P for each perturber gas in Fig. 3a (CH_3I/Ar), b (CH_3I/N_2) and c (CH_3I/CO_2). The linearity of these plots is indeed striking, as was also the case for CH_3I/SF_6 [10]. (An analysis of photoionization peak heights as opposed to peak areas gives rise to plots identical in shape to those shown in Fig. 3.)

Since the subthreshold photoionization structure is superimposed upon a rising

Table 2.
Peak areas (by gaussian fits to the photoionization spectra) for the subthreshold photoionization structure of 5.0 mbar CH_3I in varying number densities ρ (10^{19} cm^{-3}) of N_2.

ρ	11d	12d	13d	14d
0.12	0.0686	0.234	0.434	0.596
0.25	0.0823	0.241	0.475	0.645
0.49	0.101	0.290	0.545	0.769
0.73	0.128	0.313	0.602	0.868
1.22	0.159	0.412	0.744	1.10
2.50	0.285	0.598	1.09	
Regression Coefficients				
b_0	0.0574	0.215	0.397	0.541
b_1	0.0910	0.153	0.285	0.449

The regression coefficients are for a least-squares linear fit, $b_1 \rho + b_0$, as shown in Fig. 3b.

Table 3
Peak areas (by gaussian fits to the photoionization spectra) for the subthreshold photoionization structure of 5.0 mbar CH_3I in varying number densities ρ (10^{19} cm^{-3}) of CO_2.

ρ	11d	12d	13d	14d
0.12	0.0906	0.309	0.504	0.731
0.37	0.120	0.358	0.561	0.852
0.73	0.165	0.401	0.689	0.997
1.10	0.183	0.472	0.805	1.20
1.46	0.213	0.531	0.906	
Regression Coefficients				
b_0	0.0778	0.289	0.467	0.673
b_1	0.104	0.166	0.301	0.475

The regression coefficients are for a least-squares linear fit, $b_1 \rho + b_0$, as shown in Fig. 3c.

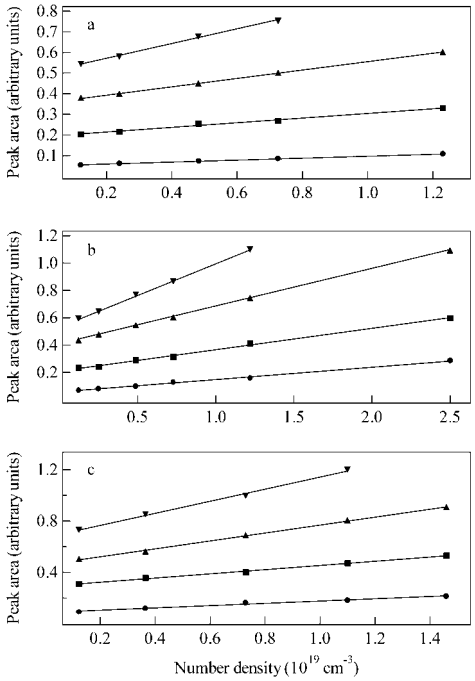

Fig. 3. Peak areas (by gaussian fits to the photoionization spectra) for the subthreshold photoionization structure of 5.0 mbar CH_3I doped into a, Ar [cf. Fig. 2]; b, N_2; c, CO_2 as a function of number density ρ (10^{19} cm^{-3}). ●, 11d; ■, 12d; ▲, 13d; ▼, 14d. The solid lines represent a least-squares fit to the function $b_1 \rho + b_0$ (cf. Tables 1-3).

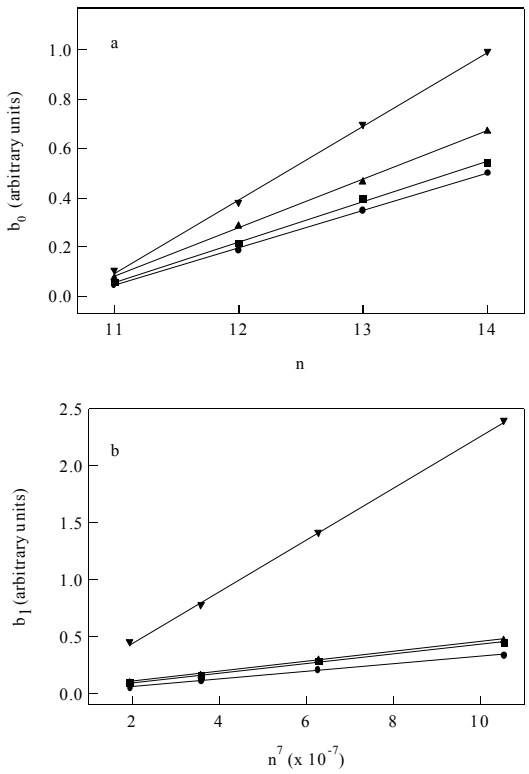

Fig. 4. (a) Constant and (b) linear regression coefficients for the subthreshold photoionization density dependence of CH_3I in varying perturbers versus the CH_3I excited state principal quantum number n and n^7, respectively. ●, Ar (Table 1); ■, N_2 (Table 2); ▲, CO_2 (Table 3); ▼, SF_6 [10]. The solid lines represent a least-squares linear fit to the data. See text for discussion

exponential background (cf. Figs. 1,2), as discussed by Ivanov and Vilesov [11,12], we have subtracted an exponential background fitted to the zero baseline and the sharp photocurrent step at threshold. The resulting spectra, when analyzed for peak area (or peak height), yield plots identical in shape to those shown in Fig. 3.

As discussed in the introduction, b_0 should scale as n (since k_1 scales as n [10]), while b_1 should scale as n^7 (since k_2 scales as n^7 [10]), where n is the principal quantum number for the CH_3I excited state. In Fig. 4, we have plotted b_0 versus n and b_1 versus n^7 for the Ar, N_2 and CO_2 data presented here, and have compared these plots to our earlier results for SF_6 [10]. Clearly, Figs. 3 and 4 demonstrate that the mechanisms of electron attachment and associative ionization are sufficient to explain the observed density dependence and n dependence of the subthreshold photoionization structure in Ar, N_2 and CO_2, as was also the case for CH_3I/SF_6 [10].

In summary, we have presented pressure-dependent subthreshold photoionization spectra of CH_3I doped into Ar, N_2 and CO_2. We demonstrated a linear dependence on perturber number density for the dopant subthreshold photocurrent signal. We then analyzed these dependences within a model that invoked both (saturated) electron attachment and associative ionization and found that the data are consistent with a perturber-stabilized Hornbeck-Molnar [16] mechanism leading to subthreshold photoionization in all cases. (Nevertheless, as mentioned in the case of CH_3I/SF_6 [10] and as originally pointed out by Ivanov and Vilesov [12], only a mass analysis of photoproducts will conclusively resolve this issue.) Finally, the subthreshold ionization effective rate constants k_1 and k_2, in terms of the regression coefficients b_0 and b_1, respectively, were shown to depend in simple ways upon the excited state of the dopant.

For Ar, N_2 and CO_2 perturbers we invoked electron attachment to form CH_3I^- [eq. (8)], while for SF_6 we invoked electron attachment to form SF_6^- [eq. (1)]. Clearly, the mechanism of eq. (8) must be present in the case of SF_6 as well, but perhaps only as a minor contributor. In order to separate these two mechanisms by the methods employed here, other dopants must be considered. (For example, ethyl iodide (CH_3CH_2I) doped into these same perturbers exhibits subthreshold photocurrent structure only for the SF_6 perturber [21].) In addition, measurements of subthreshold photoionization

intensities as a function of ρ_D, for fixed ρ_P, for various dopants and perturbers will be required to assess the general applicability of eq. (10). Such studies are currently in progress by us.

Acknowledgments

This work was carried out at the University of Wisconsin Synchrotron Radiation Center (NSF DMR-9531009) and was supported by grants from the National Science Foundation (CHE- 9506508) and from the Louisiana Board of Regents Support Fund (LEQSF (1997-00)-RD-A-14).

References

1. A. M. Köhler, R. Reininger, V. Saile and G. L. Findley, Phys. Rev. A **33**, 771 (1986).
2. A. M. Köhler, R. Reininger, V. Saile and G. L. Findley, Phys. Rev. A **35**, 79 (1987).
3. I. T. Steinberger, U. Asaf, G. Ascarelli, R. Reininger, G. Reisfeld and M. Reshotko, Phys. Rev. A **42**, 3135 (1990).
4. U. Asaf, W. S. Felps, K. Rupnik and S. P. McGlynn, J. Chem. Phys. **91**, 5170 (1989).
5. A. M. Köhler, Ph.D. thesis, Hamburg University, 1987 (unpublished).
6. J. Meyer, R. Reininger, U. Asaf and I. T. Steinberger, J. Chem. Phys. **94**, 1820 (1991).
7. U. Asaf, I. T. Steinberger, J. Meyer and R. Reininger, J. Chem. Phys. **95**, 4070 (1991).
8. U. Asaf, J. Meyer, R. Reininger and I. T. Steinberger, J. Chem. Phys. **96**, 7885 (1992).
9. C. M. Evans, R. Reininger and G. L. Findley, Chem. Phys. Letters **297**, 127 (1998).
10. C. M. Evans, R. Reininger and G. L. Findley, Chem. Phys. **241**, 239 (1999).
11. V. S. Ivanov and F. I. Vilesov, Opt. Spectrosc. **36**, 602 (1974) [Opt. Spektrosk. **36**, 1023 (1974)].
12. V. S. Ivanov and F. I. Vilesov, Opt. Spectrosc. **39**, 487 (1975) [Opt. Spektrosk. **39**, 857 (1975)].
13. S. Trajmar and J. W. McConkey, Adv. At. Mol. Opt. Phys. **33**, 63 (1994).
14. J. W. Gallagher, E. C. Beaty, J. Dutton and L. C. Pitchford, J. Phys. Chem. Ref. Data **12**, 109 (1983).
15. T. F. Gallagher, *Rydberg Atoms* (Cambridge Univ. Press, Cambridge, 1994).
16. J. A. Hornbeck and J. P. Molnar, Phys. Rev. **84**, 621 (1951).
17. J. O. Hirschfelder, C. F. Curtiss and R. B. Bird, *Molecular Theory of Gases and Liquids* (John Wiley, New York, 1964).
18. A. Rosa and I. Szamrej, J. Phys. Chem A **104**, 67 (2000).
19. A. K. Al-Omari and R. Reininger, J. Chem. Phys. **103**, 506 (1995).
20. K. N. Altmann, A. K. Al-Omari and R. Reininger, Chem. Phys. Letters **261**, 597 (1996).
21. C. M. Evans, R. Reininger, J. D. Scott, F. H. Watson and G. L. Findley, in preparation.